JOURNAL OF GEOPHYSICAL RESEARCH, VOL. 100, NO. B9, PAGES 17,837–17,854, SEPTEMBER 10, 1995

Northeastern Pacific mantle conductivity profile from long-period magnetotelluric sounding using Hawaii-to-California submarine cable data

Daniel Lizarralde

Massachusetts Institute of Technology/Woods Hole Oceanographic Institution, Woods Hole, Massachusetts

Alan Chave and Greg Hirth

Department of Geology and Geophysics, Woods Hole Oceanographic Institution, Woods Hole, Massachusetts

Adam Schultz

Institute of Theoretical Geophysics, University of Cambridge, Cambridge, England

Abstract. We present results of a long-period magnetotelluric (MT) investigation of the electrical structure beneath the eastern North Pacific. The electric field data consist of ~2 years of continuously recorded voltages across an unpowered, ~4000-km-long submarine telephone cable (HAW-1) extending from Point Arena, California, to Oahu, Hawaii. The electric field measurements are coherent to some degree with magnetic field measurements from Honolulu Observatory at periods of 0.1 to 45 days. This coherence is enhanced at long periods over that observed with point electric field sensors due to horizontal averaging of the motional electric fields of spatial scale smaller than the cable length, significantly diminishing their effect. Robust, controlled leverage MT response estimates and their jacknife confidence limits are computed for the HAW-1 to Honolulu data. An equivalent scalar MT response obtained from Honolulu magnetic variations data is used to correct the HAW-1 MT response for static shift and to extend the MT response estimate to periods of 100 days. The composite response function satisfies necessary and sufficient conditions for consistency with a one-dimensional conductivity structure and is most sensitive to structure between 150 and 1000 km. Inversion of the MT response reveals a conductive zone (0.05-0.1 S/m) between 150 and 400 km depth and a positive gradient below 500 km; these observations are consistent with previous MT studies in the North Pacific. This upper mantle conductivity is too high to be explained by solid-state conduction in dry olivine using reasonable mantle geotherms. Calculations based on measurements of hydrogen solubility and diffusivity in olivine indicate that H^+ dissolved in olivine, possibly combined with a lattice preferred orientation consistent with measured seismic anisotropy, provide sufficient conductivity enhancement to explain the inversion results. The high conductivity may also be explained by the presence of gravitationally stable partial melt. Comparison of the HAW-1 results with long-period MT studies conducted on land reveals differences in upper mantle conductivity between different tectonic regimes. In particular, the upper mantle beneath the Pacific Ocean is considerably more conductive than that beneath the Canadian shield and similar in conductivity to that beneath the Basin and Range.

Introduction

Laboratory measurements of mantle rocks and mineral assemblages and results from electromagnetic induction studies demonstrate that the conductivity of Earth's mantle ranges over many orders of magnitude. Mantle conductivity is sensitive to a variety of factors including temperature, presence of volatiles and fluids, and oxygen fugacity [e.g., *Schock et al.*, 1989; *Karato*, 1990; *Constable et al.*, 1991; *Duba and Constable*, 1993]. Knowledge of the conductivity structure of the mantle can thus provide information on the physical state of the mantle which has not been revealed by seismology, the principle source of our current knowledge of mantle properties.

Paper number 95JB01244.
0148-0227/95/95JB-01244$05.00

In this paper, we present the results of an unconventional long-period magnetotelluric investigation of the electrical structure beneath the eastern North Pacific. The magnetotelluric (MT) method uses surface or seafloor measurements of electric and magnetic field fluctuations to make inferences about the conductivity structure of Earth. Variations in the electric and magnetic fields recorded at the ocean floor are induced by two primary sources: fluctuations of Earth's magnetic field due to external, ionospheric and magnetospheric current systems, and the dynamo interaction of moving, conductive seawater within Earth's stationary magnetic field. External current systems provide the source fields for magnetotelluric investigation. The motionally induced fields are of interest for oceanographic investigations [e.g., *Chave and Luther,* 1990] but represent a long-period noise source for MT work.

The time-varying electric field measurements used in this study consist of nearly 2 years of continuous recordings obtained from a decommissioned, unpowered submarine telephone cable

extending from Hawaii to California. *Chave et al.* [1992] discuss analyses of the initial year of measurements from this system and show that horizontal averaging of the electric field over the cable length significantly diminishes the size of motionally induced fields at periods of 1-10 days or more. The averaging property of the cable and the ease with which long duration records are obtained represent advantages over seafloor point-sensor measurements for deep soundings of mantle conductivity. These advantages come at the expense of lateral spatial information within the lithosphere.

In addition, we use geomagnetic depth sounding (GDS) measurements to extend the bandwidth of the MT response to periods of 100 days, enabling the resolution of conductivity to depths of ~1000 km. Other recent long-period MT studies by *Egbert et al.* [1992] and *Schultz et al.* [1993] that also combine conventional MT methods with longer-period GDS measurements have demonstrated the improving ability of electromagnetic methods to resolve mantle structure. These studies, based on data from the Basin and Range and the Canadian craton, respectively, also suggest significant lateral variability in mantle conductivity. The results presented here extend the database of deep mantle conductivity profiles to an oceanic environment.

Data Analysis

Measurements of the time-varying electric field used in this study were obtained from the decommissioned Hawaii-1 (HAW-1) system which is based on AT&T 1950s seabed cable technology. The HAW-1 system consists of a parallel pair of unpowered, submarine telephone cables separated north-south by ~120 km and extending from Hanauma Bay, Oahu, Hawaii (21°16'N, 157°42'W), to Point Arena, California (38°59'N, 123°42'W), at an azimuth of ~42° with respect to geomagnetic north (Figure 1). Details of the data collection system are given by *Lanzerotti et al.* [1992]. Only data from the northern cable are considered here, as the southern cable was broken in 1991 about 200 km off Hawaii, presumably by a submarine landslide. The electric potential time series used in this study was decimated to 20-min values from the original 2-s samples beginning April 7, 1990, and ending December 5, 1992. The time series contains several short data gaps representing 2.4% of the total. The geomagnetic data consist of hourly mean values of three-component magnetic field measurements made at the Honolulu Observatory (HON) during calendar years 1990 and 1991 as reported by the U.S. Geological Survey (USGS). The magnetic component data contain gaps representing 3.6% of the time series samples.

Preprocessing of the electric and magnetic field time series consisted of removal of harmonic components due to the quasi-periodic solar daily variation (S_q) of fundamental period 1 day, harmonics of S_q at 2, 3, 4, 5, 6, 7, and 8 cpd, and the eight largest ocean tides. Estimates of the amplitude and phase of sinusoids at these periods and the record mean were made by robust least squares for each time series component. Up to five additional sidebands at multiples of 1 cycle per year about each S_q component frequency were also fit to grossly account for seasonal modulation effects. These signals violate the usual source field assumptions of magnetotellurics [cf. *Egbert et al.*, 1992] and were subtracted from the time series to reduce the potential for spectral leakage into nearby frequency bands. In Figure 2a we show 1 month of the HAW-1 electric field data, the periodic signal subtracted from it, and the resulting S_q- and tide-corrected time series. The HAW-1 data were then low-pass filtered and decimated to hourly mean values to match the magnetic field data.

Multiple-Window Spectra and Coherences

Several interesting aspects of the HAW-1 data are revealed by computation of spectra and coherences at the longest possible periods. This requires that time series gaps first be filled in a physically consistent manner. The methodology we used to fill data gaps has been described by *Egbert* [1992] and is similar to that used by *Chave et al.* [1992] in their analyses of the initial year of HAW-1 data. For each HAW-1 and HON time series component to be corrected, a multivariate frequency domain transfer function with jacknife error estimates relating the gappy data component to all three components of a reference magnetic field was computed using a robust method [*Chave and Thomson,* 1989]. Fresno geomagnetic observatory data were used as a reference for the HON data, and HON was used as a reference for HAW-1. Inversion of these transfer function estimates to obtain a time domain impulse response was performed using a regularization approach. Of those impulse responses whose Fourier transforms fit the estimated transfer function to within the speci-

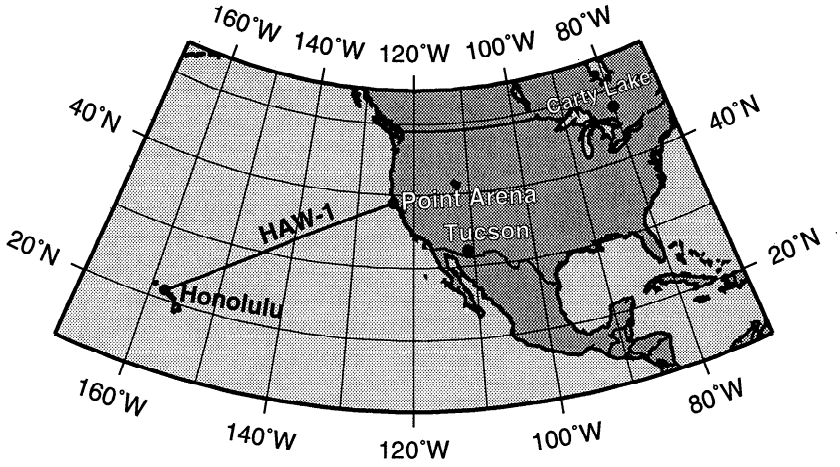

Figure 1. Map showing locations of HAW-1 cable and recent long-period MT studies at Tucson [*Egbert and Booker*, 1992] and Carty Lake, Ontario [*Schultz et al.*, 1993].

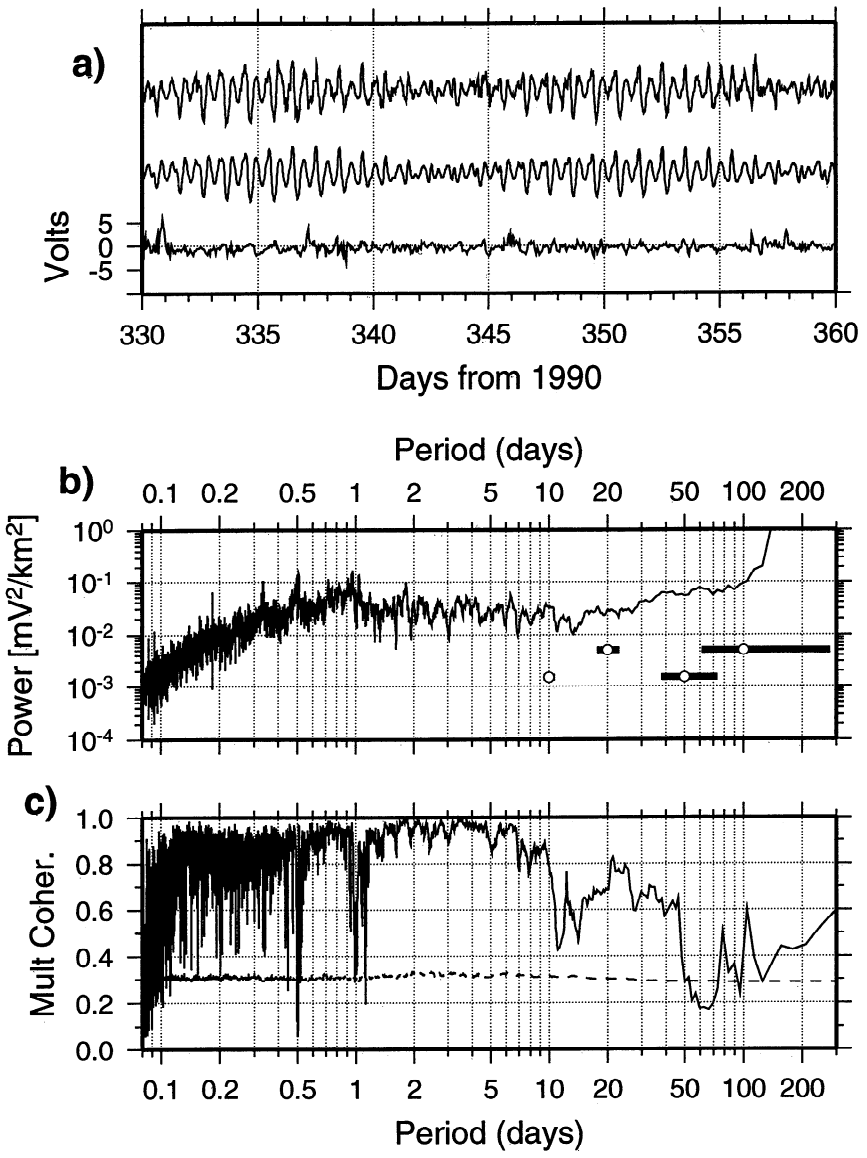

Figure 2. (a) (top) One month of the HAW-1 electric field time series, (middle) sinusoids fit to the data at S_q and tidal periods, and (bottom) HAW-1 data corrected for S_q and ocean tides. (b) Multiple window power spectrum of the first 625 days of the detided, gap-filled HAW-1 time series computed using eight time-bandwidth-product 4 eigenspectra. The estimates have a resolution bandwidth of ~0.012 cpd at each frequency and possess ~14 degrees of freedom. The band-width is indicated at periods of 10, 20, 50 and 100 days by the bold lines with open circles. (c) Multiple coherence between the HAW-1 and HON time series, with the zero confidence coherence indicated as a dashed line.

fied error level, the one with the smoothest Fourier transform with respect to log frequency is chosen. Time series gaps were filled by convolution of the reference time series with the time domain impulse responses computed in this manner. We note that gappy data sections were not used in the computation of the MT response function; thus the MT response function is not affected by this type of processing.

The multiple window power spectrum [*Thomson,* 1982] computed for the HAW-1 time series is shown in Figure 2b. The resolution bandwidth of ~0.012 cpd is indicated by the bold lines at periods of 10, 20, 50, and 100 days (open circles). Power increases smoothly with period up to 1 day, is flat between 1 day and 10 days, and again increases very slowly with period beyond 10 days. The negative slope between 10 and 100 days is resolved given the resolution bandwidth of the estimates. The HAW-1 spectrum is in contrast to spectra of point sensor electric field measurements in which power tends to rise rapidly with increasing period above ~1 day due to the influence of small spatial scale oceanic sources [*Chave et al.,* 1992]. The multiple coherence for the HAW-1 and HON data is shown in Figure 2c with the zero coherence level at 95% significance indicated by a dashed line. Strong multiple coherence is indicated to periods of 10 days followed by an abrupt drop in coherence just beyond 10 days and then a return to moderate values near periods of 20 to 45 days.

Response Function Estimation

For sufficiently uniform external sources and in the absence of noise, the electric and magnetic fields measured at Earth's surface

may be related by the linear expression

$$\mathbf{E}=\mathbf{ZB} \quad (1)$$

where **E** and **B** are the horizontal components of the electric and magnetic fields in the frequency domain and **Z** is a complex second rank tensor referred to as the MT response or impedance tensor which contains information about the electrical structure of Earth [cf. *Larsen,* 1970; *Egbert and Booker*, 1989]. The HAW-1 data represent an integral along the cable length of only one component of **E**, E_y. For a sufficiently one-dimensional conductivity structure, however, the potential measured by the cable is equivalent to E_y multiplied by a known factor. Furthermore, for a sufficiently one-dimensional conductivity structure, $Z_{yx} \approx -Z_{xy}$ and $Z_{yy} \approx Z_{xx} \approx 0$, and the inability to obtain the Z_{yx} and Z_{yy} components of **Z** presents no difficulties for further analyses. We consider the requirements on the dimensionality of the conductivity structure in the following section.

The response function and associated standard error for the HAW-1 and HON data were determined using section-averaged, robust estimation techniques and the nonparametric jacknife described by *Chave et al.* [1987], *Chave and Thomson* [1989], and *Thomson and Chave* [1991]. These tech-niques reduce the influence of data outliers and local nonstationarity on the MT response and error estimates [e.g., *Jones et al.*, 1989]. A number of window lengths were used to estimate the response, as the robust estimation method is most efficient at frequencies near one over the segment length. The time series were first prewhitened using a five-point autoregressive filter and then, for a given window length, were broken up into a number of 50% overlapping data segments. These segments were multiplied by a time-bandwidth 1 Slepian sequence [*Thomson*, 1977], transformed into the frequency domain, and the magnetic field data were rotated into a coordinate system whose y axis points toward the northeast in the direction of the HAW-1 cable. Samples at S_q and its harmonic frequencies were rejected to avoid source field contamination. Robust regression methods were then ap-plied to the section spectra, with slight additional band averaging to achieve an even logarithmic spacing of 10 estimates per decade. For a given window length T, transfer function estimates at frequencies of a few times $1/T$ were chosen for the response.

The real and imaginary parts of the estimated principal response Z_{yx}, the jacknife standard errors δZ_{yx}, and the magnitude of the diagonal term $|Z_{yy}|$ are listed in Table 1. We note that $|Z_{yy}|$ is small relative to $|Z_{yx}|$. The principal response is shown in Figures 3a and 3b in the form of apparent resistivity ρ_a and phase ϕ with approximate double-sided 95% confidence limits computed by multiplying the first-order Taylor series expansion of ρ_a and ϕ

$$\delta\rho \approx 0.4\, T\, |Z_{yx}|\, |\delta Z_{yx}| \quad (2)$$

$$\delta\phi \approx \sin^{-1}(|\delta Z_{yx}| \,/\, |Z_{yx}|) \quad (3)$$

by 1.96, where T is the period in seconds. Also shown in Figures 3a and 3b are equivalent MT response function estimates computed from band-averaged B_z/B_x transfer function estimates based on ~60 years of HON observatory data [cf. *Schultz and Larsen,* 1983; *Schultz* , 1990]. We will refer to these estimates as the GDS (geomagnetic depth sounding) response. The GDS response was used to correct the HAW-1 response for static shift, presumably associated with noninductive galvanic distortion of the electric field which does not affect the GDS response [*Larsen*, 1977; *Chave and Smith*, 1994]. A frequency-independent multiplicative factor of 0.5 was applied to the HAW-1 response to correct for static shift, aligning the HAW-1 and GDS responses. A clearer understanding of the source of the static shift will be obtainable in the near future now that a Hawaii-to-Midway submarine cable has come online, providing a north-south electric field component and enabling decomposition of the full distortion tensor. A composite HAW-1/GDS response extending from 0.178 to 100 days period (Figures 3d and 3e) was formed by removing redundant data points from the overlapping region near 5 days.

One-Dimensional Inversion of Response Functions

The inversion of imperfect MT data for conductivity is non unique. We use a combination of several one-dimensional (1-D) inversion techniques to verify the appropriateness of a 1-D model

Table 1. Real and Imaginary Parts of Z_{yx} of the HAW-1/HON Impedance Tensor as a Function of Period

Period, days	Re[Z_{yx}], mV km nT^{-1}	Im[Z_{yx}], mV km nT^{-1}	δZ_{yx}, mV km nT^{-1}	Degrees of Freedom	$\lvert Z_{yy} \rvert$ mV km nT^{-1}
0.17778	8.52784	16.59841	0.37815	3596.00	1.87981
0.24242	8.16669	14.36923	0.31420	3596.00	2.51014
0.33333	7.87218	12.50012	0.32307	1798.00	2.86487
0.44444	6.58427	10.83065	0.30140	1798.00	1.92714
0.66667	5.12088	9.79991	0.26963	819.02	2.02673
0.88652	4.09803	8.98729	0.33094	486.67	0.98891
1.42222	2.63903	5.93172	0.27185	376.02	0.59826
1.93939	1.94396	5.34900	0.20150	358.91	1.03732
2.66667	1.74281	4.10488	0.25118	182.79	0.72468
3.55556	1.44238	3.32857	0.25145	177.12	0.73596
5.20833	0.67140	2.27087	0.33286	84.85	0.28402
7.57576	0.28185	1.73277	0.23264	63.91	0.31422
10.41667	0.54040	0.82782	0.46965	31.30	0.57706

Also given are standard error, degrees of freedom for the estimate, and magnitude of the Z_{yy} component.

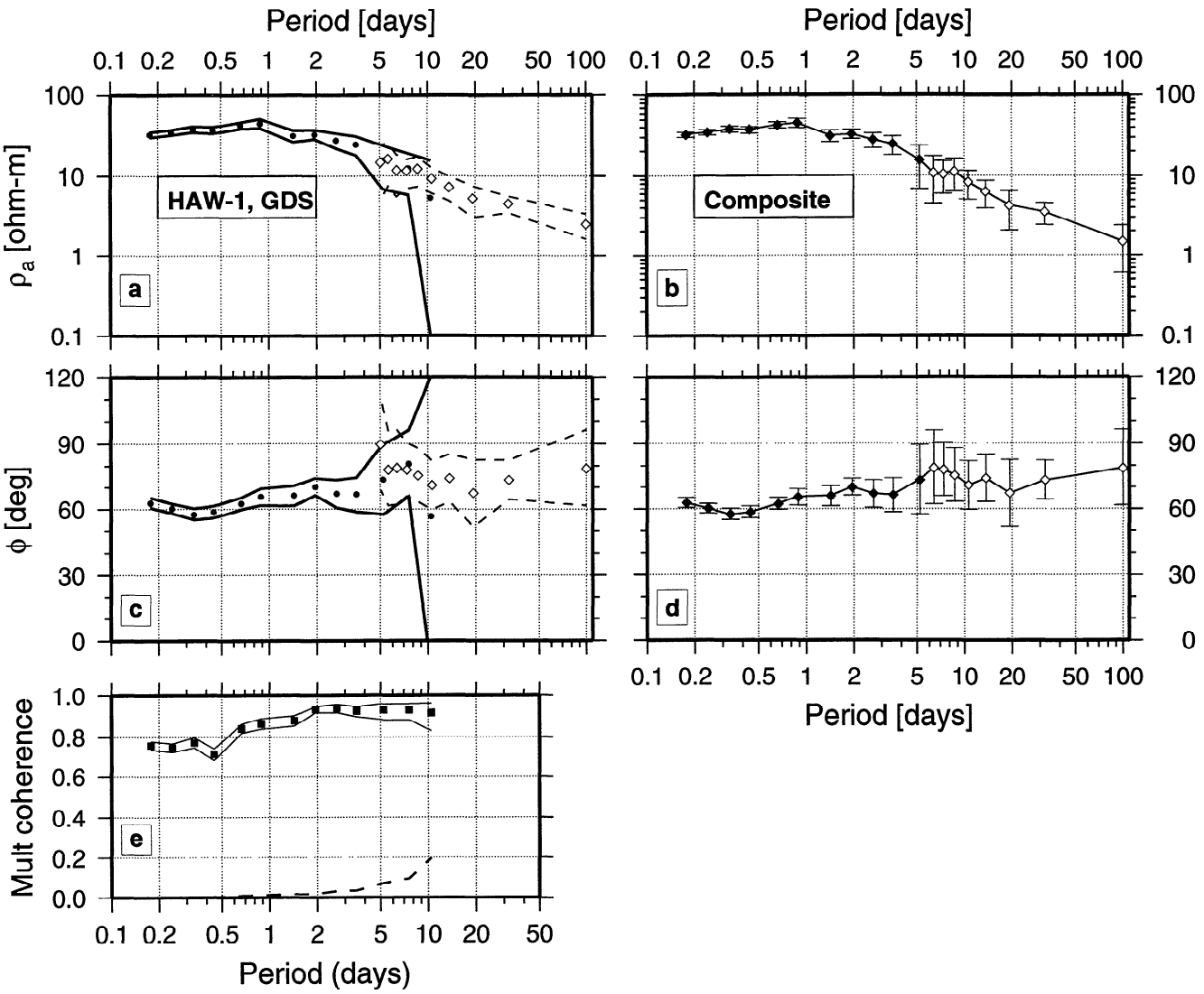

Figure 3. (a) Apparent resistivity of the HAW-1/HON Z_{yx} (HAW-1) (dots and solid line) and GDS (diamonds and dashed) response functions with double-sided 95% confidence bounds. (b) Apparent resistivity of composite HAW-1/GDS response. (c) Phase of the HAW-1 and GDS responses with confidence bounds. (d) Phase of the composite response. (e) The multiple coherence for the HAW-1 response with 1σ bounds and zero confidence coherence (dashed line).

and then to place constraints on conductivity models which satisfy the data. We use the D^+ algorithm of *Parker and Whaler* [1981] to establish consistency of the data with a 1-D structure. We then use the Flat 1-D algorithm of *Smith and Booker* [1988] to invert for the conductivity model having a minimum amount of structure while being consistent with the data and its errors. Finally, we use an extensive search of H^+ model space [*Parker and Whaler*, 1981] and a nonlinear recombinant genetic analog algorithm [*Everett and Schultz*, 1993] to test for the possible existence of features not resolved by the minimum structure inversion and to assess the strict requirement for features that are resolved by the minimum structure inversion.

D^+ and Minimum Structure Inversion

Parker [1980] has shown that for imprecise data, the best fitting 1-D conductivity model is drawn from a model space consisting of a set of infinitesimally thin sheets of finite conductance separated by perfect insulators, the D^+ model space. The ability of the D^+ inversion to obtain a 1-D model that satisfactorily fits the data establishes necessary and sufficient conditions for consistency of a response function with a 1-D conductivity structure [*Parker*, 1980]. The criterion for the fit is based on the standard χ^2 misfit statistic

$$\chi^2 = \sum_{i=1}^{2N} \left[\frac{r_i}{\varepsilon_i} \right]^2, \tag{4}$$

where r_i are the residuals from the fit, ε_i are the data standard errors, and N is the number of complex pairs in the response function being fit. We accept only models that fit the data to within two standard errors of the expected value of χ^2, i.e., $E[\chi^2]+2\sigma$, which is approximately the 95% point of χ^2. Both the GDS and the composite HAW-1/GDS response functions satisfy this criterion (Table 2). The D^+ criterion is not satisfied when response estimates at periods less than 0.18 day are included, presumably due to magnetic field galvanic distortion at these periods. These

Table 2. Fit Statistics of Inversion Runs

Response Function	D^+			Flat 1-D			
	$E[\chi^2]+2\sigma$	χ^2	Z_{max}, km	$\chi^2(-1/c)$	$\chi^2(c)$	$P(H_1)$	n
GDS	30.00	4.26	920	30.00	34.68	.484	-1.0
MT/GDS	55.43	32.61	980	55.00	55.80	.120	-1.5

Z_{max} is the maximum inference depth below which a perfectly conducting half space does not appreciably affect the model response, $P(H_1)$ is the probability that the hypothesis that no trend exists in the data residuals is true, and n is the power of $(z_o+z)^n$.

shorter-period estimates were thus not included in the composite response.

The D^+ inversion result establishes consistency of the composite response with a 1-D conductivity structure. It does not, however, prove that the entire impedance tensor is consistent with a 1-D structure. Such a proof is not possible at present due to the single-component nature of the electric field data. We note again that the Z_{yy} component of the impedance tensor is smaller than the Z_{yx} component by a factor of ~7. This fact, in combination with the D^+ result, strongly suggests that a 1-D interpretation of the MT response is both sufficient and appropriate.

Having established consistency with a 1-D structure, we then inverted the response functions using the Flat 1-D algorithm of *Smith and Booker* [1988], a linearized inversion that seeks the flattest 1-D conductivity structure consistent with the data and its errors. Minimum structure inversion provides a means for making inferences based on a model that does not uniquely satisfy the data. We may be reasonably confident, for example, that structure exhibited by the flattest model consistent with the data is in fact required by the data. The minimum structure model is obtained by minimizing a roughness penalty function of the form

$$\Phi = \int_0^\infty \left[\frac{d\log(\sigma(z))}{df(z)} \right]^2 df(z) \qquad (5a)$$

where

$$\frac{df(z)}{dz} = (z+z_0)^n \qquad (5b)$$

subject to the constraint that the data be fit to some selected level. As a fit criterion we chose only models that fit the data to within two standard errors of the expected value of χ^2. Additionally, we required that the fit to the data be "white" in the sense that all frequencies are fit equally well. Fitting either the higher or lower frequencies preferentially may result in unnecessary structure in either the shallow or deeper parts of the model. As a whiteness criterion we used the robust Spearman's D statistic to test the significance of trends in the residuals, following *Smith and Booker* [1988]. If the residuals of a given model did not satisfy the D statistic criterion, the exponent n on (z_0+z) in (5) was adjusted and the inversion rerun. The exponent n essentially governs over which portion of the conductivity profile structure is penalized most; values of n=0, -1, and -2 correspond to models that are flattest with respect to z, $\log(z)$, and z^{-1}.

Results of the D^+ and Flat 1-D inversions are summarized in Figure 4 for the composite HAW-1/GDS response function and Figure 5 for the GDS response alone. Statistics on these results are listed in Table 2. In Figures 4a and 5a we plot the resolving kernels of the Flat 1-D inversion at selected center depths. In Figures 4b and 5b we indicate the D^+ inversion results as vertical bars of finite conductivity, scaled from the finite conductance delta functions of the D^+ model by dividing by the midpoint distances, and the results of the Flat 1-D inversion as 2σ statistical error bars about each model parameter. Figures 4c and 4d and 5c and 5d indicate the real and imaginary parts of the inductive scale length, $c(\omega)=iZ(\omega)/\omega$ (open circles), that were jointly inverted, 1σ error bars on $c(\omega)$, and the predicted response of the Flat 1-D model (solid diamonds). In Figures 4e and 5e we plot the residuals for the real (solid squares) and imaginary (open diamonds) parts of $c(\omega)$ and indicate the modulus of the residual as a line passing through the 1σ error bars of the c values. It is the modulus of the residuals that were required to satisfy the D statistic criterion.

Analyses by *Smith and Booker* [1988] and *Egbert and Booker* [1992] suggest that for minimum structure MT inversion with $\log(\sigma)$ as a model, linearization errors may be small enough to interpret the minimum structure model as the truth smoothed through the computed resolution kernels and that the resolution kernel centered at z_o may be interpreted as the fractional contribution from the true conductivity at depth z to the smoothed (model) conductivity at z_o. The resolving kernels shown for the HAW-1/GDS Flat 1-D inversion (Figure 4a) are centered at 100, 200, 300, 400, 600, 800, 1000, 1200, and 1400 km. These kernels are peaked in the 150-300 km and 600-1000 km intervals, indicating good resolution in these regions. Poor resolution in the 300-600 km interval indicates that structure in this region may be masked by the high conductivity above. The resolution kernels shown for the GDS response inversion are centered at 500, 900, and 1500 km and indicate that the GDS response is most sensitive to conductivity structure in the mid-mantle.

The D^+ and Flat 1-D inversion results for the HAW-1/GDS response suggest an interval of increased conductivity in the 150-300 km depth interval possibly followed by a decrease and a positive gradient below 500 km. The GDS inversion results indicate a positive gradient below ~300 km, and there is a conductivity delta function from the D^+ inversion located at 0 km depth (shown at 1 km in Figure 5). *Schultz and Larsen* [1990] and *Schultz* [1990] discuss analyses of a HON GDS response with a nearly identical D^+ result. Both studies interpret the shallow conductance as related to enhanced upper mantle conductivity, although *Schultz* [1990] maintains the possibility that a fraction of the surface conductance may be due to the presence of conducting seawater. The addition of the HAW-1 data has resulted

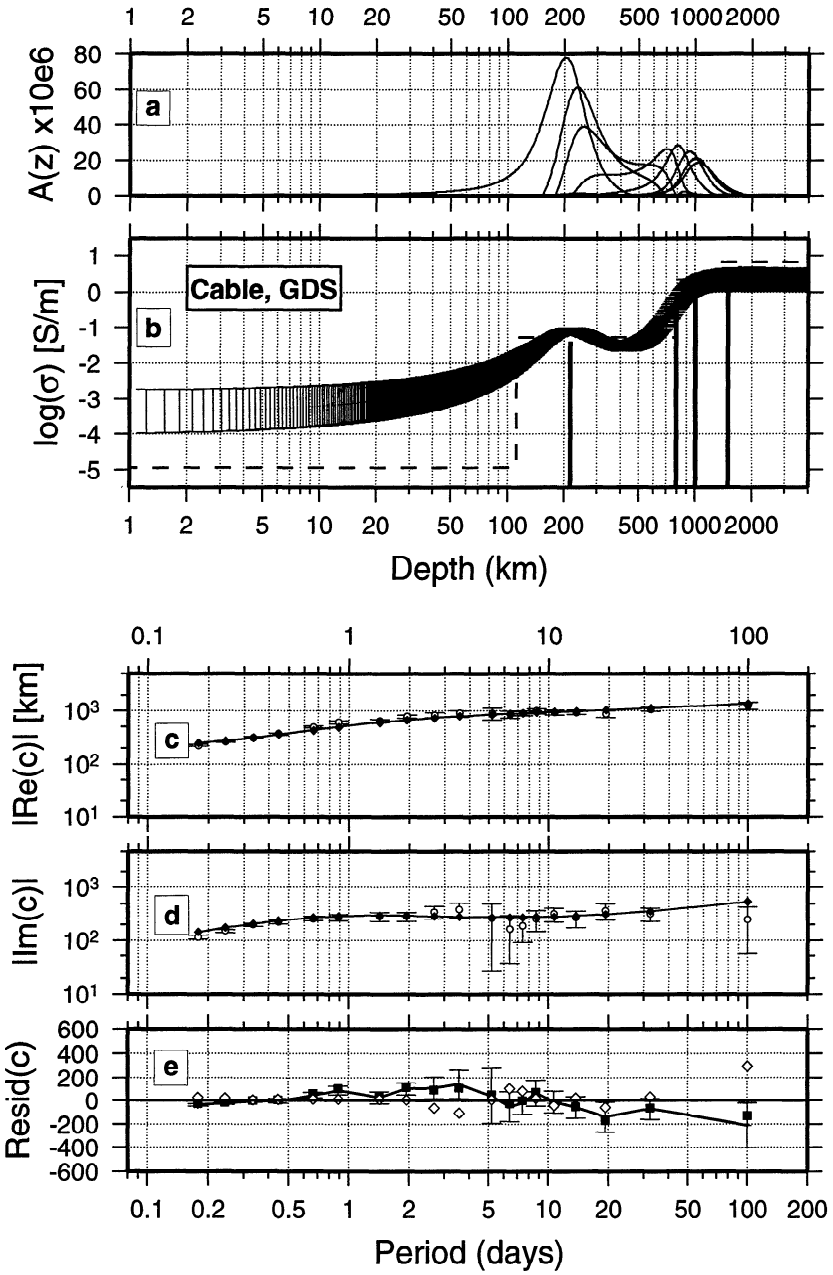

Figure 4. Results of D^+ and Flat 1-D inversion of composite HAW-1/GDS response. (a) Resolving kernels of the linearized Flat 1-D inversion centered at 200, 300, 400, 500, 600, 700, 800, 1000, 1200, and 1400 km. (b) Vertical bars of finite conductivity scaled from finite-conductance deltas of the D^+ model by dividing by the midpoints between them; result of the Flat 1-D inversion indicated by 2σ statistical error about model parameters; and layered RGA model indicated by dashed line. (c) Real and (d) imaginary parts of the c values (open circles) with 1σ error bars and the predicted response (solid diamonds) of the Flat 1-D model. (e) Residuals for the real (solid squares) and imaginary (open diamonds) parts of $c(\omega)$ and the modulus of the residual (line passing through the 1σ c value error bars).

in the localization, at upper mantle depths of 150-300 km, of the shallow conductance required by GDS data alone.

H^+ and RGA Hypothesis Testing

The H^+ model space consists of layered models for which each layer has the same value of the layer parameter $d^2 = \mu_0 \sigma h^2$ (where μ_0 is magnetic permeability, σ is conductivity, and h is layer thickness). The results of an extensive search of H^+ model space with varying d^2 are shown in Figure 6. H^+ models exist that fit the HAW-1/GDS response to within 2σ of $E[\chi^2]$ with values of $d^2 \leq 42{,}750$ s. Smaller values of d^2 are associated with more rapid diffusion times through Earth and can be attributed to finer-scale structure in the mantle. There are zones within Earth where, in H^+ model space, conductive layers are found, and these correspond to those con-ductive zones in the minimum structure inversion model. One difference between the H^+ and D^+ results is that by choosing a suitable range of layer parameters, it is possible to distribute the conductance of the shallowest D^+ delta function into a layer spanning depths between approximately 150 and 400 km. The HAW-1/GDS data do not require any fine-scale,

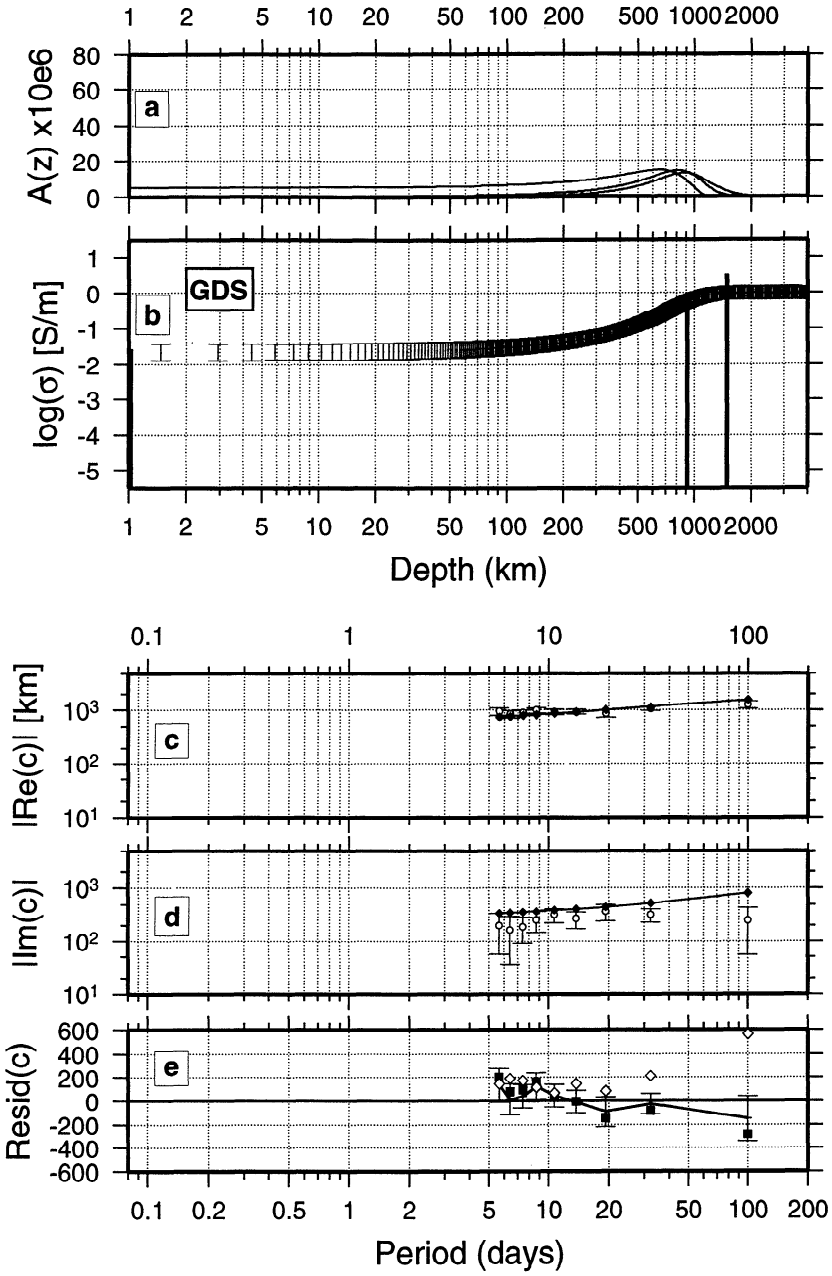

Figure 5. Results of D^+ and Flat 1-D inversion of the GDS response. Legend same as in Figure 4 but with resolving kernels centered at 500, 900, and 1500 km.

localized conductivity jumps. In contrast, data from a deep MT sounding in the Canadian Shield strictly require localized conductivity jumps in the upper mantle [*Schultz et al.*, 1993].

We then used the recombinant genetic analog (RGA) nonlinear inversion algorithm of *Everett and Schultz* [1993] for hypothesis testing on the HAW-1/GDS data. The method is based on a modified form of a genetic algorithm using prior bounds. We have parameterized the earth into 13 homogenous layers of finite conductivity and thickness. As a control, an initial nonlinear model search was conducted where the a priori bounds on the conductivity and thickness for all layers were $10^{-5} \leq \sigma \leq 10^{1}$ S/m and $1 \leq h \leq 500$ km. A population of 56 random models was used, and rapid convergence to an acceptable model ($\chi^2 \leq E[\chi^2]+2\sigma$) was seen.

We then tested two hypotheses. The first is motivated by the minimum structure inversion which suggests that there exists a localized zone of high conductivity at 150-300 km depth, with a negative gradient below 200 km followed by a positive gradient below 500 km; a view reinforced by the H^+ inversion results. We thus tested the hypothesis that a nonmonotonic depth dependence of conductivity is strictly required by the data. We used the identical a priori bounds as taken for the control inversion for all 13 layers within the model and imposed an additional constraint by modifying the norm. Rather than using the χ^2 misfit as the objective function, we weighted this misfit measure by the first derivative of the conductivity with respect to depth and imposed a positivity constraint on that derivative such that only models with monotonically increasing conductivity with depth are deemed acceptable.

With these constraints imposed, a layered Earth model with monotonically increasing conductivity with depth was found with a χ^2 misfit of 51.13, less than $E[\chi^2]+2\sigma$. This model, shown as a

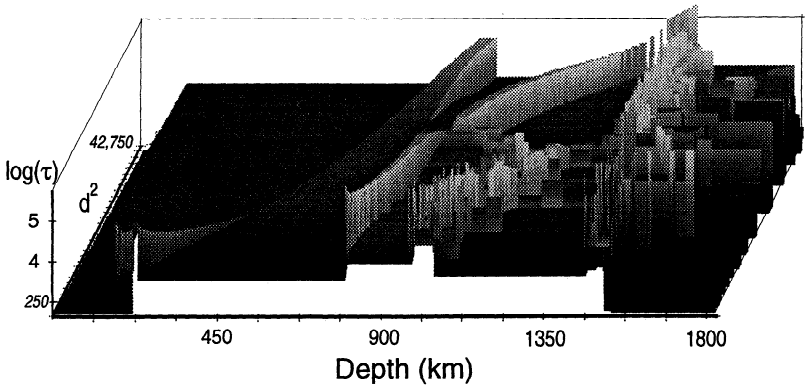

Figure 6. Full range of best fitting H^+ layered earth models found to fit the HAW-1/GDS complex $c(\omega)$ response values to a χ^2 misfit of 55.4.

dashed line in Figure 4b, appears as a linear approximation to the minimum structure model. The fit of the RGA model is not white, however, with higher frequencies being preferentially fit. Inversion runs with the additional constraint of whiteness-of-fit failed to produce monotonic models which adequately fit the data. It is therefore not possible to strictly reject the hypothesis that a high conductivity layer is required by the data. For this reason, and because of its more realistic parameterization, we tend to prefer the minimum structure model over the RGA model. We emphasize, however, that the two models exhibit essentially the same large-scale conductivity features and that arguments based on the nonmonotonicity of the minimum structure model should be avoided.

Finally, we tested for the existence of a major difference between upper mantle conductivity determined for the Pacific from the HAW-1 MT data and that determined for the Canadian shield by the MT study of *Schultz et al.* [1993]. These data suggest a significantly more conductive upper mantle beneath the Pacific than beneath the Canadian shield. We tested the hypothesis that a model exists with a priori bounds for the two uppermost mantle layers which correspond to the shallowest two delta functions found within the best fitting D^+ model for the Canadian shield MT data; specifi-cally $5\text{x}10^{-4} \le \sigma \le 5\text{x}10^{-2}$ S/m and $229 \le h \le 231$ km for the uppermost layer and $5\text{x}10^{-4} \le \sigma \le 5\text{x}10^{-3}$ S/m and $189 \le h \le 191$ km for the layer immediately beneath it. By carrying out a nonlinear model search with these delta functions imposed on the solution, it is possible to determine if any model exists that fits the HAW-1 data which also contains the shallowest conduc-tive features found to be required beneath the Canadian Shield. No model of this sort was found to fit the data, strengthening the suggestion that the upper mantle beneath this part of the Pacific and that beneath the Canadian shield differ in a fundamental way.

Modeling of Coastal Effects

We have examined the response of simple two-dimensional (2-D) models to investigate the possible effect of the North American coast on our MT results and to further assess the suitability of a 1-D model. A finite difference code based on a network formulation of the Maxwell equations [*Madden*, 1972] was used to calculate the response of the conductivity models. Our intention here is only to show gross consistency or inconsistency with end-member conductivity structures and not to present rigorous 2-D models of northeastern Pacific electrical structure. In particular, we address the recently debated concern that a strong coastal effect due to an electrically isolated ocean basin precludes the application of 1-D interpretations of seafloor MT data [*Heinson and Constable*, 1992], a conclusion which is controversial [*Tarits et al.*, 1993; *Constable and Heinson*, 1993]. We suggest that the HAW-1 MT response is not consistent with an electrically isolated ocean basin bounded by resistive continents and oceanic lithosphere and that this implies substantial leakage of current through the resistive upper mantle between the ocean and deep mantle somewhere in the structure.

The magnitude of the coast effect depends largely on the resistivity of the lithospheric mantle and the presence of conductive pathways into the less resistive mantle beneath. A resistive upper mantle inhibits current leakage into the more conductive mantle below, resulting in a strong coast affect [cf. *Bullard and Parker*, 1968; *Ranganayaki and Madden*, 1980]. We first consider the conductivity models of Figure 7a (model A), a 1-D model based on the Pacific Ocean reference model of *Chave et al.* [1990] between 0 and 100 km depth and our results below 100 km; and Figure 7b (model B), a 2-D model formed from model A and the 2-D model of *Mackie et al.* [1988] for coastal California. The resistive oceanic upper mantle of models A and B is based on a controlled-source electromagnetic (CSEM) study in the Pacific Ocean [*Cox et al.*, 1986] and MT studies in California [*Mackie et al.*, 1988]. The thickness and lateral extent of this resistive layer are poorly constrained. However, if these resistivities are correct to an order of magnitude, we would expect strong coast-effect distortion of the HAW-1 response.

The results of the response function calculation for models A and B are shown in Figure 8 along with the HAW-1/GDS response. The light lines correspond to apparent resistivity and phase at each seafloor node (i.e., the response that would be seen by a point-sensor located at that node), and the heavy line with dots corresponds to the integrated response seen by a cable extending from the coast 4000 km seaward computed using the magnetic field at the seaward end of the cable, as for the HAW-1 response. The 1-D model A without coastlines fits the data approximately as well as the Flat 1-D inversion model. The predicted response for model B underfits the HAW-1 apparent resistivity by roughly a factor of 10. This result indicates that the HAW-1 data are not consistent with a strong coast effect in an electrically isolated ocean basin and suggests that current leakage out of the ocean basin is taking place via some conductive pathway.

MT studies near continental margins and magnetometer array

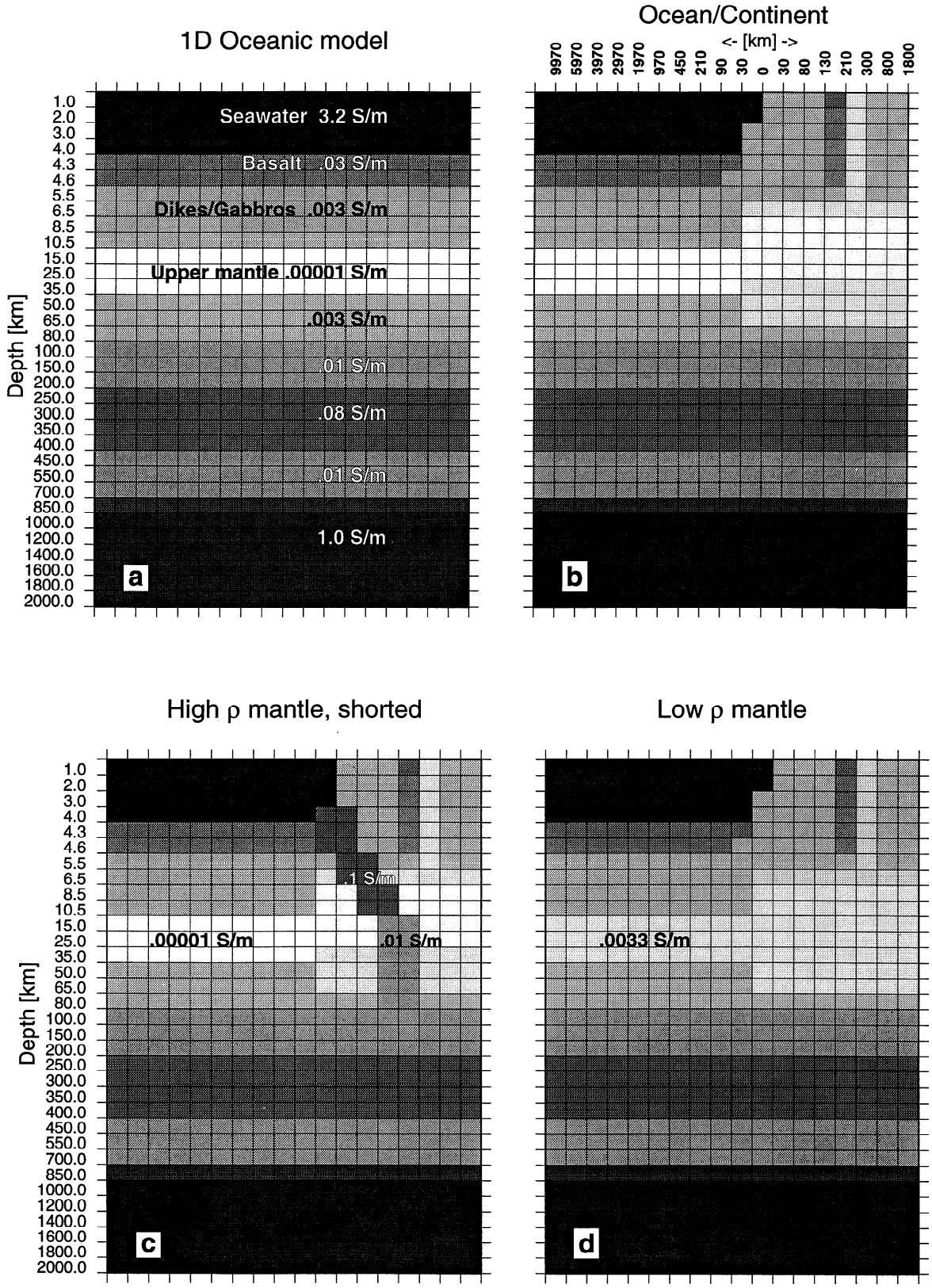

Figure 7. Conductivity models for the northeastern Pacific. (a) One-dimensional model based on our results and the Pacific Ocean reference conductivity model of *Chave et al.* [1990]. (b) Two-dimensional model formed from Figure 7a and the 2-D coastal California model of *Mackie et al.* [1988], distances in km from the coast correspond to node positions. (c) 2-D model of Figure 7b with a "short circuit" through the resistive mantle. (d) 2-D model of Figure 7b with upper mantle resistivities reduced by a factor of 33 in the ocean and 3 in the continent.

studies in several regions suggest that subduction zones and crustal sutures provide vertical electrical connections through the upper mantle [*Gough,* 1989; *Wannamaker et al.*, 1989; *Kurtz et al.*, 1990; *Park et al.*, 1991]. In Figures 7c and 7d we show two models based on model B in which the conductance of the lithospheric mantle has been increased, in model C by adding a conductive pathway or "short circuit" through the resistive mantle near the coastline and in model D by reducing upper mantle resistivities by a factor of 33 in the ocean and 3 in the continent. We note that in model C the vertical conductance of ~250 S is chosen to be consistent with that determined by *Park et al.* [1991] for inferred crustal-suture conductivity in California and by *Wannamaker et al.* [1989] for the upper edge of the subducting Juan de Fuca plate. Mid-ocean ridges, such as the nearby Gorda Rise, represent likely analogs for model D, in which wholesale reduction in upper mantle resistivities may occur. The integrated responses predicted by these two models (Figure 9) are both sufficiently near the observed values to suggest that either mechanism alone may sufficiently diminish the coastal effect and explain the HAW-1 observations. It is possible that a combination of these mechanisms operate over the ocean basin to increase the effective conductance of the lithosphere, though it is not possible to differentiate between them with a long seabed cable. Thus the extremely resistive upper lithosphere detected by *Cox et al.* [1986] is not a pervasive feature of the ocean basin.

Discussion

The principal results of this study are the conductivity models shown in Figure 4. The dominant features of these profiles are a conductive zone (0.05-0.1 S/m) between ~150 and 500 km and positive gradient below ~500 km leading to higher conductivities at depth. Two main conclusions follow from these results. (1) The conductivity of the northeastern Pacific upper mantle is elevated relative to that of a dry olivine mantle. (2) The conductivity of the northeastern Pacific upper mantle is elevated relative to that in stable continental regions, suggesting a fundamental heterogeneity between oceanic and continental upper mantle.

As demonstrated in Figure 10a, our result is in general agreement with previous MT studies in the northeast Pacific which have resolved mantle electrical structure down to ~400 km depth [*Filloux,* 1980; *Chave et al.,* 1981]. We also plot in Figure 10a an empirically determined model for the conductivity of dry olivine at upper mantle temperatures and pressures, the SO2 (standard olivine 2) model of *Constable et al.* [1991]. Mantle temperatures were estimated using *Parson and Sclater's* [1977] cooling plate model for a 110-km-thick, 70 Ma plate and an adiabatic geotherm of 0.28°C km^{-1} below 110 km. It has previously been observed, and is ob-served again here, that unrealistically high temperatures are required to explain the high upper mantle conductivity determined from MT data by solid-state conduction

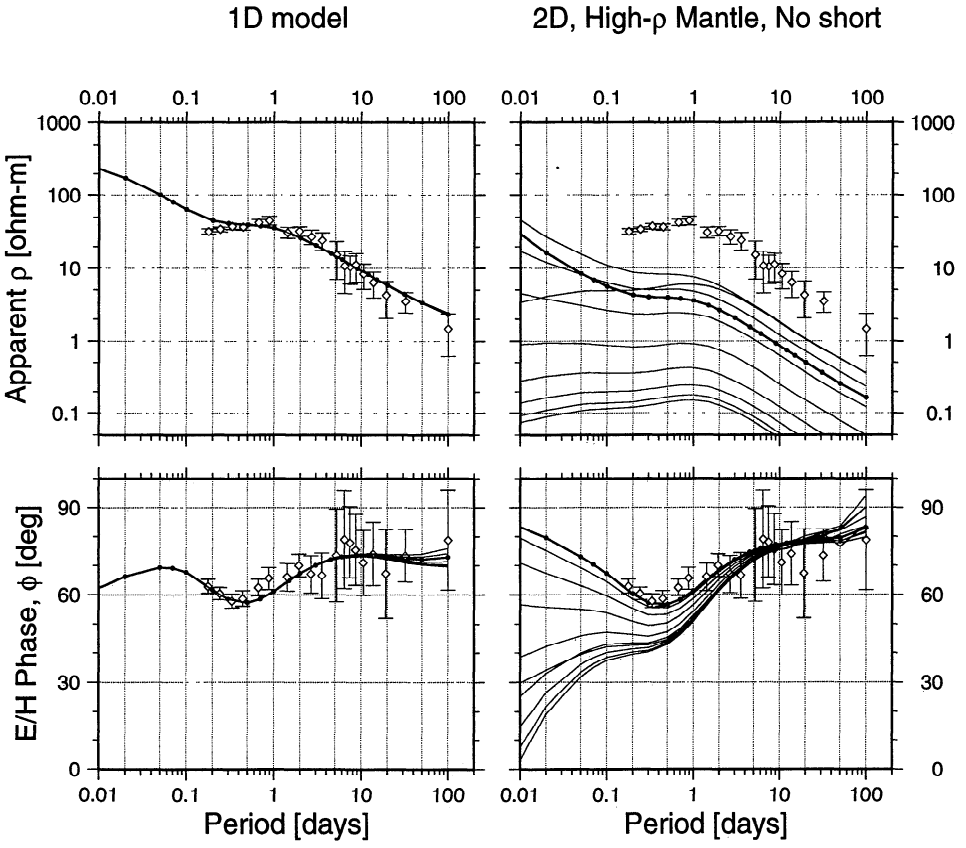

Figure 8. Results of the response function calculation for models shown in Figures 6a and 6b. HAW-1/GDS composite response function (open diamonds) with 1σ error bars is indicated. Light lines correspond to ρ_a and ϕ at each node at the seafloor, heavy line with dots corresponds to the integrated response seen by a cable extending from the coast seaward 4000 km computed using the magnetic field at the seaward end of the cable.

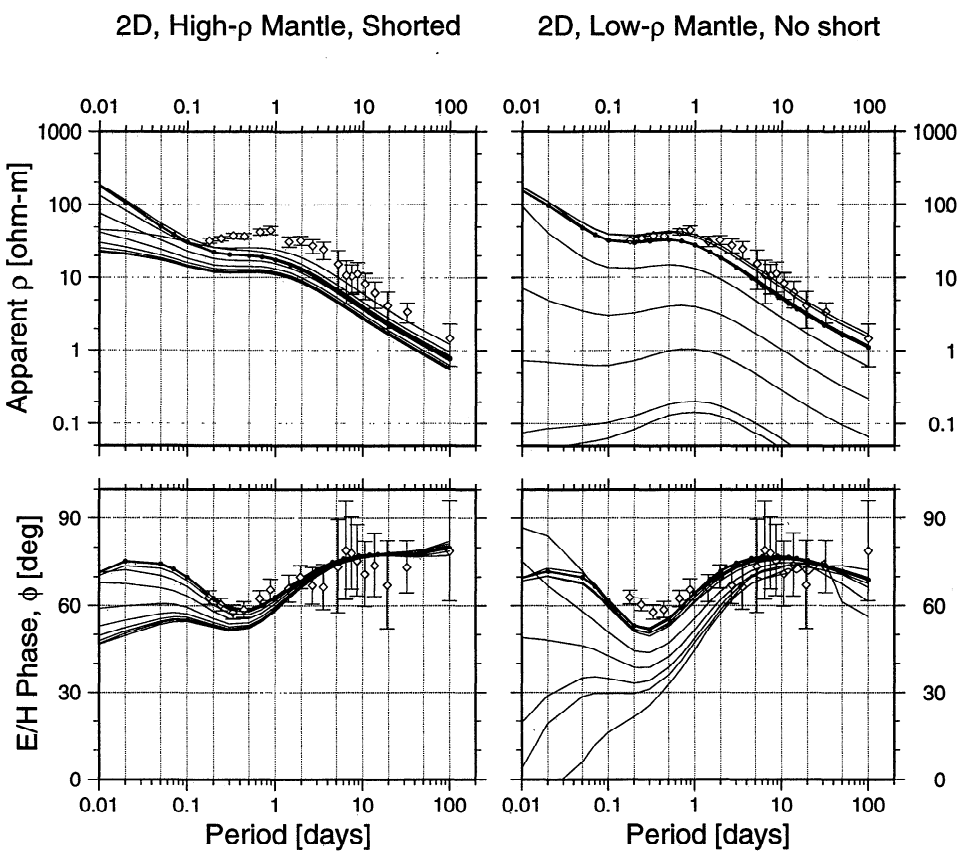

Figure 9. Predicted responses of models shown in Figure 7c and Figure 7d. Format is the same as in Figure 8.

in dry olivine. This conclusion is equally valid with the monotonic model of Figure 4.

The inability of dry olivine to explain the MT results has led, on the one hand, to the proposal of mechanisms that enhance conductivity such as partial melt and dissolved hydrogen or other volatiles [e.g., *Waff*, 1974; *Karato*, 1990] and, on the other, to the suggestion that the MT results are biased by distortion due to coastal effects [*Heinson and Constable,* 1992]. The latter suggestion is partially motivated by the notion that the proposed enhancement mechanisms require unreasonable mantle conditions. For example, *Constable and Heinson* [1993] argue that gravitational instability of interconnected melt in the mantle [*McKenzie*, 1985] precludes the accumulation of volumetrically significant melt networks, and *Constable* [1993] argues that the H^+ solubility required to explain the MT results by dissolved hydrogen seems too large when an appropriate effective medium average of anisotropic H^+ diffusivity in olivine is considered. We have shown above that our data are not consistent with a strong coast effect. Below we illustrate how water-derived hydrogen may enhance mantle conductivity relative to that predicted for dry olivine and demonstrate that the MT results may be explained by this mechanism under reasonable mantle conditions. We also consider the possibility that gravitationally stable melt may be present in the upper mantle and the implications of our results for the volume and conductivity of such a phase.

Effect on Conductivity of Water Dissolved in Nominally Anhydrous Mantle Minerals

Analyses of water contents in mantle derived xenoliths and experimentally annealed specimens of olivine indicate that nominally anhydrous mantle minerals may act as important reservoirs for water in the mantle [e.g., *Bell and Rossman*, 1992; *Bai and Kohlstedt*, 1992]. The presence of water in the mantle may act to increase mantle conductivity in several ways, by supplying mobile charge carriers in the form of H^+ ions [*Karato*, 1990], by enhancing the mobility of existing charge carriers [D. L. Kohlstedt, submitted manuscript, 1994], or by reducing melting temperatures below the adiabat and introducing a more conductive melt phase into the system. Sufficient laboratory measurements of olivine and melt conductivity exist to enable simple modeling of some of these effects. We consider the effect on conductivity of two cases, the presence of dissolved water-derived hydrogen and the presence of devolitization-induced partial melt.

We examine the maximum influence of dissolved water-derived hydrogen on mantle conductivity by considering the conductivity of olivine at the H^+ solubility limit and assuming that this volumetrically dominant phase is interconnected and controls mantle conductivity. Following *Karato* [1990], we use the Nernst-Einstein relation, which relates ionic conductivity to carrier concentration and mobility [e.g., *Kittel*, 1957, p. 486], to determine the contribution of mobile H^+ ions to the electrical conductivity of olivine,

$$\sigma = c\, D\, q^2 / kT \qquad (6)$$

where c is the ionic concentration, D is the ionic diffusivity, q is the ionic charge (here equal to the electron charge $+e$), k is Boltzman's constant, and T is absolute temperature. An estimate of the maximum concentration of water-derived hydrogen as a

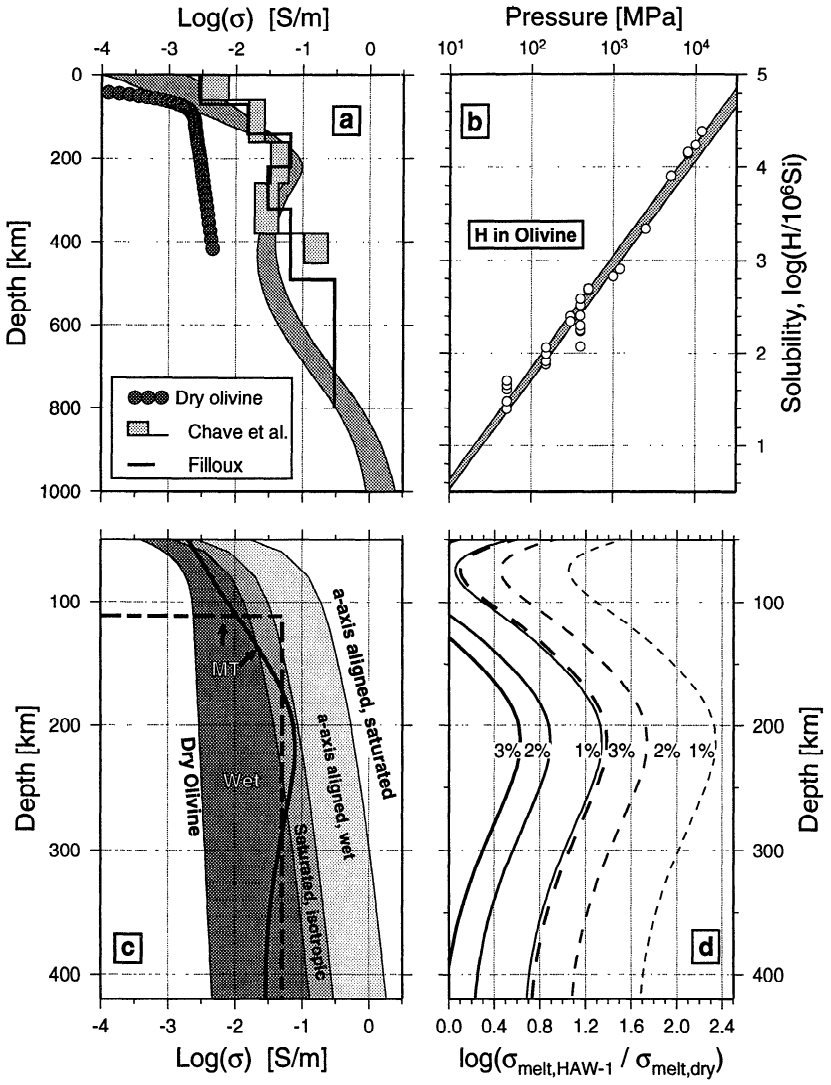

Figure 10. (a) The minimum structure model of Figure 4 with the seafloor MT results of *Filloux* [1980] and *Chave et al.* [1981] overlain. Also indicated is the predicted conductivity for dry olivine (the SO2 model of *Constable et al.* [1991]). (b) Least square error fit to the hydrogen solubility data of *Bai and Kohlstedt* [1992] and D. L. Kohlstedt (unpublished data, 1994). (c) Effects of water and *a* axis alignment on conductivity of an olivine mantle. Hashin-Shtrikman bounds for saturated, isotropic olivine define central region; the bounds for dry, isotropic olivine (the SO2 model of *Constable et al.* [1991]) and saturated, a-axis-aligned olivine define a region of "mixing" between conductivity enhancement due to lattice-preferred orientation and water. The MT results (heavy lines) may be explained solely by the presence of water or by a combination of undersaturated and anisotropic conditions. (d) Conductivity enhancement required to satisfy the HAW-1 results assuming 1, 2, and 3% partial melt and Archie's law behavior with a porosity exponent of 1.5 (solid lines) and 2.0 (dashed lines).

function of depth may be obtained from the solubility measurements of *Bai and Kohlstedt* [1992], taken at 1300°C and pressures of 0.05, 0.15, and 0.3 GPa, with hydrogen fugacity ranging from $10^{0.5}$ to $10^{3.2}$ at each pressure, and measurements up to ~12 GPa at 1100°C [*Kohlstedt et al.*, 1994]. The solubility data are well fit by a linear regres-sion of log($H^+/10^6$ Si) versus log(pressure), as shown in Figure 10b. A least squares fit yields

$$[H^+]_{ppm\ Si} = 10^{-0.61\pm0.04}\ P^{1.19\pm0.01}\ (\text{MPa}) \quad (7)$$

The influence of pressure on solubility arises from at least two sources: (1) the dependence of water fugacity (and therefore oxygen and hydrogen fugacity) on pressure and (2) compression of the olivine lattice at higher pressures. The lower-pressure experiments of *Bai and Kohlstedt* [1992] demonstrate an approximately linear dependence of water solubility on water fugacity. This linear correlation breaks down at high pressures, where the water fugacity coefficient increases rapidly, indicating an additional negative pressure dependence presumably due to compression of the olivine lattice [*Kohlstedt et al.*, 1994].

Measurements of the diffusivity of water-derived hydrogen in olivine are reported by *Mackwell and Kohlstedt* [1990] for temperatures between 800° and 1000°C and pressures of 0.30 GPa. *Mackwell and Kohlstedt* [1990] demonstrate that diffusion of hydrogen in olivine is anisotropic, with diffusion along each of the crystallographic directions (a, b, c) following an independent Arrhenius relationship

$$D_a=(6\pm3)\times10^{-5}\exp[-(130\pm30)/RT]$$
$$D_c=(5\pm4)\times10^{-6}\exp[-(130\pm30)/RT] \quad (8)$$
$$D_b\approx.01D_a\,.$$

We evaluate (6) for the principal crystallographic axes of olivine over a depth range of 60-550 km using (7) and (8), the geotherm described above, and pressure values from *Anderson* [1989, p. 387]. In these calculations we assume no pressure dependence for the diffusivity and no temperature dependence for either the solubility of (7) or the activation enthalpy, the numerator of the exponential term in (8). *Karato* [1990] argues that the small activation enthalpy of (8) implies a small activation volume, and thus a weak pressure dependence. The assumption of no temperature dependence for the activation energy yields a minimum estimate for conductivity as activation energies often increase with rising temperature. Similar arguments hold for the temperature dependence of solubility.

Following *Shankland and Duba* [1990], we compute Hashin-Shtrikman bounds on conductivity (the narrowest bounds on a two-phase medium in the absence of geometric considerations [*Hashin and Shtrikman*, 1962; *Waff*, 1974]) for a homogenous, isotropic effective medium consisting of parallel and series averages of the crystal axis conductivities. These bounds are plotted in Figure 10c as defining the region of conductivity for saturated, isotropic olivine. In addition, we plot the conductivity of dry, isotropic olivine (the SO2 model of *Constable et al.* [1991]) and the conductivity of an olivine aggregate with a lattice preferred orientation defined by an *a* axis lineation that is horizontal and parallel to the HAW-1 cable direction and hence approximately parallel to the paleospreading direction of the Pacific plate. The bounds for dry, isotropic olivine and saturated, anisotropic olivine define a region of "mixing" between conductivity enhancement due to *a* axis alignment and water saturation. Thus the region defined by the Hashin-Shtrikman bounds for the maximum conductivity of an isotropic, water-saturated olivine mantle may also be explained by an undersaturated olivine mantle with some *a* axis alignment.

As demonstrated in Figure 10c, the HAW-1 MT results may be explained by an isotropic upper mantle nearly saturated in hydrogen (or water) or by a combination of mantle anisotropy and undersaturated conditions. The likelihood of such mantle conditions must be considered in the context of current views of oceanic lithosphere evolution. It is currently believed that the evolution of northeastern Pacific oceanic lithosphere involved passive upwelling and decompression melting of mantle beneath a fast spreading center and passive mantle flow away from the ridge crest [cf. *Forsyth*, 1992; *Parmentier and Phipps Morgan*, 1990]. These processes result in a horizontally stratified mantle in which the upper ~100 km [*Salters and Hart*, 1989] is depleted in incompatible trace elements (including water) due to melt extraction. In addition, mantle flow away from the spreading center is thought to result in the development of a lattice preferred orientation of olivine grains [cf. *Nicolas and Christensen*, 1987]. Results of seismic surface wave studies in the Pacific reveal seismic anisotropy consistent with horizontal *a* axis olivine alignment in the direction of spreading that persists to depths of ~200 to 250 km [*Cara and Leveque*, 1988; *Nishimura and Forsyth*, 1989].

The evidence for upper mantle seismic anisotropy suggests the presence of conductivity anisotropy which persists to depths of ~200 to 250 km. If this is the case, then the results of Figure 10c imply that the upper mantle is undersaturated in water, as would be expected for a depleted upper mantle. Water contents below maximum depths of melting, however, may resemble those of the mid-ocean ridge basalt (MORB) source region. The water content near 200 km depth implied by Figure 10c for anisotropic conductivity (~$10^{3.1}$ H/10^6Si) matches geochemical estimates of water contents in the MORB source region [*Michael*, 1988; *Bell and Rossman*, 1992] and is considerably less than the solubility limit defined by the data of Figure 10b ($10^{3.8}$–$10^{4.0}$ H/10^6 Si). Below 200 km, the MT-determined conductivity falls below the Hashin-Shtrikman bounds for a saturated mantle and thus may be explained by an undersaturated, isotropic mantle. This is equally true for both the minimum structure and the RGA models. Thus the MT results may be explained by a depleted, anisotropic mantle above 200 km and an increasingly isotropic mantle below 200 km with undersaturated concentrations of water.

Gravitationally Stable Melt With Conductivity Enhancement Due to the Presence of Water

The results of *Agee and Walker's* [1988, 1993] studies of molten komatiite and peridotite compression have recently been used to argue for the presence of gravitationally stable melt within the lowermost upper mantle [e.g., *Revenaugh and Sipkin*, 1994; *Nolet and Zielhuis*, 1994]. Agee and Walker show that komatiite melts are more dense than olivine at pressures above ~8 GPa, or ~250 km depth in Earth. These results suggest that melt produced in the upper mantle below ~250 km may tend to remain in place or sink. The presence of melt would likely enhance upper mantle electrical conductivity.

The production of melt below 250 km depth requires some combination of volatiles and increased temperature. The higher solubility of water in β-Mg_2SiO_4 than in olivine [*Young et al.*, 1993; *Kohlstedt et al.*, 1994] led *Thompson* [1992] to propose that the peridotite solidus may be driven below the adiabat by dehydration of mantle upwelling above 410 km. The depth extent of the resulting melting event, the composition of the melt produced, and the ability of pyroxenes to inhibit such an event are all unclear as the equilibrium conditions for the peridotite-H_2O-melt system are not known at these pressures. It is possible that melt produced in such a setting will be gravitationally stable, and it is likely that water will strongly partition into the melt [*Bell and Rossman*, 1992].

The presence of water in melt may significantly increase its conductivity by providing a more mobile charge carrier, as described above for olivine, or by enhancing the diffusivity of existing charge carriers. Data pertaining to these effects at relevant P-T conditions are sparse. The data that do exist, however, suggest a relationship between conductivity enhancement and dissolved H_2O in melt. For example, ionic and oxide diffusivities of silicate melts have been shown to increase by orders of magnitude due to the presence of dissolved H_2O in experiments conducted at temperatures below 1000°C and pressures below 3 kbar [*Chekhmir and Epel'baum*, 1988; *Watson*, 1979, 1981]. In addition, the results of *Keppler and Bagdassarov* [1993] provide direct evidence for high proton mobility in a rhyolite melt containing 300 ppm (by weight) H_2O at temperatures up to 1300°C and atmospheric pressure.

We investigate the amount of conductivity enhancement required to explain our results in terms of both percent melt and enhancement to the conductivity of the melt. We consider a two-phase mantle consisting of dry olivine and dry tholeiitic basalt, and use the SO2 model of *Constable et al.* [1991] and the results of *Tyburczy and Waff's* [1983] experiments on dry tholeiitic basalt

to constrain the conductivities of these phases (equations (9) and (10)). While it is unlikely that a partial melt in the lower part of the upper mantle would produce a tholeitic basalt, these are the best suited available data for this analyses. The conductivity of the two-phase medium is modeled using equation (11), a modified form of Archie's law [cf. *Schmeling*, 1986]

$$\sigma_{solid}=10^{2.402}\, e^{-1.60\ eV/kT}+10^{9.17}\, e^{-4.25\ eV/kT} \quad (9)$$

$$\sigma_{melt,dry}=10^{5.332}\, e^{-1.533\ eV/kT} \quad (10)$$

$$\sigma=\sigma_s+(\sigma_m-\sigma_s)(\text{melt fraction})^n. \quad (11)$$

Following the arguments of *Heinson and Constable* [1992], we consider a value of the melt fraction exponent n=2 a realistic lower bound on electrical conductivity for a given porosity, and a value n=1.5 appropriate for the upper mantle. Using both values (n=1.5 and 2.0), the geotherm described above, melt fractions of 0.01, 0.02, and 0.03, and (10), we solve (11) for the melt conductivity required to explain the HAW-1 MT results, $\sigma_{melt,HAW-1}$. The ratio $\sigma_{melt,HAW-1}/\sigma_{melt,dry}$, which represents the amount of melt-conductivity enhancement required to explain the HAW-1 results, is plotted in Figure 10d.

As demonstrated in Figure 10d, melt-conductivity enhancement by a factor of ~3 (3% melt, n=1.5) to ~200 (1% melt, n=2.0) times is required to explain the HAW-1 minimum-structure inversion results. This level of water-related conductivity enhancement is similar to that predicted for solid-phase, water-saturated olivine (Figure 10c). These models demonstrate that gravitationally stable melt below 200 km depth with enhanced conductivity due to the presence of dissolved water may explain the high upper mantle conductivities observed at and below 200 km. The results of *Agee and Walker* [1993] suggest that gravitationally stable melt below 200 km is possible. The probability of such a situation requires further experimental data relating to the compressibility of melts in equilibrium with peridotite at present day lower mantle pressure-temperature conditions.

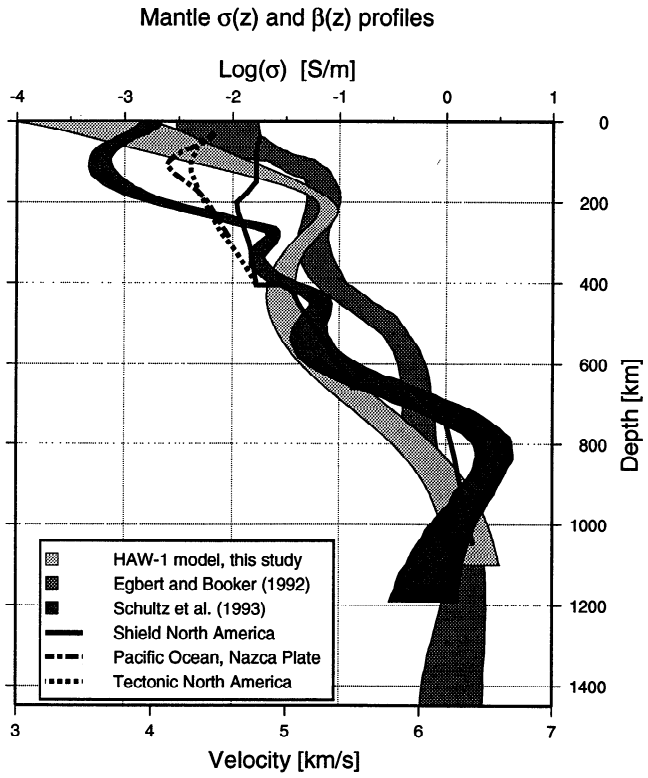

Figure 11. Comparison of HAW-1 model with models of *Egbert and Booker* [1992] and *Schultz et al.* [1993]. Locations of these studies given in Figure 1. Also indicated are shear wave velocity profiles for mantle beneath the Canadian shield, the Nazca plate, and tectonic North America.

Comparison With Other Long-Period MT Results

The explanations discussed above for the upper mantle conductivity structure determined from our MT data are uncertain, involving several assumptions and extrapolations of existing data. Explanations of conductivities determined for the transition zone and lower mantle involve even greater levels of uncertainty due to the sparse and conflicting nature of laboratory measurements on representative mineral assemblages (see the discussion by *Egbert et al.* [1992]). The possible existence of significant volatile concentrations within the transition zone presents additional complications to the interpretation of deep mantle conductivity [e.g., *Li and Jeanloz*, 1991; *Gasparik*, 1993; *Navrotsky and Bose*, 1994].

Long-period MT studies, in combination with GDS measurements, are providing better estimates of mantle conductivity in a variety of tectonic settings. In conjunction with further laboratory constraints on mantle conductivity, and particularly the role of volatiles, we may be able to constrain fundamental differences in conductivity structure between different tectonic environments. In Figure 11 we compare our minimum-structure conductivity model with minimum structure models obtained from long-period MT data at Tucson, Arizona [*Egbert and Booker*, 1992], and Carty Lake, Ontario [*Schultz et al.*, 1993] (see Figure 1 for locations). Each data set was analyzed in a similar manner using robust processing techniques. While the HAW-1 and Carty Lake MT data are both consistent with a 1-D conductivity structure, the Tucson MT data, at periods less that 1 day, are not. *Egbert et al.* [1992] demonstrate, however, that large-scale averages of mantle conductivity (i.e., conductance) are well constrained by these data and that only a small number of simple conductivity models are consistent with them.

Each of the conductivity profiles in Figure 11 is associated with a distinct tectonic setting, oceanic (HAW-1), extensional continental (Tucson), and stable cratonic (Carty Lake). The most dramatic differences between these conductivity profiles exist in the upper 300 km. Both the HAW-1 and Tucson profiles indicate high-conductivity regions between ~100 to 300 km where the Carty Lake profile indicates a conductivity low. These differences are likely related to the very different thermal regimes of oceanic and extensional tectonic versus much colder cratonic settings, as well as the greater probability for the existence of volatiles and partial melt within the upper mantle beneath the eastern Pacific and the Basin and Range.

Below 200 km, the Carty Lake and HAW-1 profiles approach one another, and below 400 km these profiles are quite similar, though Carty Lake exhibits considerably more structure. This fine scale upper mantle structure is required by the Carty Lake data [*Schultz et al.*, 1993] but is not required by the HAW-1 data, as demonstrated by the H^+ inversion. The high-conductivity zone near 400 km on the Carty Lake profile may be characteristic of the olivine/spinel transition, possibly due to a change in the partitioning of volatiles. It is possible that similar structure is present beneath the Pacific but is not resolved by the HAW-1 data which have poor resolution between ~300 and 600 km depth,

possibly due to masking of structure by the high conductivity near 200 km depth. Alternatively, the differences in conductivity structure near 400 km may reflect a fundamental heterogeneity between suboceanic and subcratonic mantle, perhaps indicative of a tectosphere beneath cratonic North America [*Jordan*, 1981].

In Figure 11 we have also plotted shear wave velocity profiles for similar tectonic settings: Pacific Ocean (PAC, the Nazca plate), tectonic North America (TNA, includes the Basin and Range), and shield North America (SNA, Canadian shield) [*Grand and Helmberger*, 1984; *Forsyth*, 1975]. The general features observed in the conductivity profiles are in agreement with similar trends over depth seen in the shear wave velocity profiles. Large differences exist between the PAC/TNA and SNA profiles between 100 and 200 km. Below 200 km the velocity profiles draw together, and below 400 km they are the same. This correlation of general features between completely independent geophysical observations suggests that long-period magnetotelluric observations can play a role of similar significance to seismic observations in elucidating mantle structure.

Conclusions

We have presented results of a long-period MT sounding based on ~2 years of continuously recorded electric field measurements from an unpowered, Hawaii-to-California submarine phone cable. The major conclusions of this work may be summarized as follows:

1. MT response estimates obtained using Honolulu geomagnetic data were combined with a GDS response for Honolulu to form a composite MT response at periods between 0.18 and 100 days. The composite response is consistent with a 1-D conductivity structure and is most sensitive to conductivity between 150 and 1000 km depth.

2. Simple 2-D modeling indicates that the MT response is not consistent with an electrically isolated ocean basin bounded by resistive continents and oceanic lithosphere.

3. Inversion of the MT response reveals a conductive zone (0.05-0.1 S/m) between 150 and 400 km depth and a positive gradient below 500 km. The upper mantle conductivity cannot be explained by solid-state conduction in dry olivine using reasonable mantle geotherms.

4. The upper mantle conductivity may be explained by water dissolved in an olivine mantle that is depleted and anisotropic (a lattice preferred orientation consistent with measured seismic anisotropy) above 200 km and, below 200 km, increasingly isotropic with undersaturated concentrations of water. It may also be explained by the presence of gravitationally stable partial melt.

5. Other recent long-period MT studies from different tectonic settings reveal significant differences between the conductivity profiles beneath oceans and cratons, particularly in the upper mantle. These differences may be related to differing thermal settings, volatile and partial melt content, and development of a tectosphere beneath the North American craton.

Acknowledgments. The efforts of Louis Lanzerotti, Les Medford, and AT&T Submarine Systems in establishing the HAW-1 system and providing the data are acknowledged and appreciated. We thank Ted Madden and Randy Mackie for providing us with their 2-D modeling code and for their insightful comments on this paper. We thank David Kohlstedt for allowing us to use his measurements of hydrogen solubility in olivine and for useful discussions. Discussions with Peter Kelemen, Karen Fischer, and Sue Circone also contributed to the ideas presented in this paper. Thoughtful reviews by V. Haak, J. Larsen, and H. Keppler have improved the paper and are appreciated. Support for this research was provided by NSF grant EAR92-18851. Woods Hole Oceanographic Institute contribution 8912. Department of Earth Sciences and Institute of Theoretical Geophysics, University of Cambridge, contribution 4306.

References

Agee, C. B., and D. Walker, Static compression and olivine floatation in ultrabasic silicate liquid, *J. Geophys. Res,. 93*, 3437-3449, 1988.

Agee, C. B., and D. Walker, Olivine floatation in mantle melt, *Earth Planet. Sci. Lett., 114*, 315-324, 1993.

Anderson, D. L., *Theory of the Earth,* Blackwell Sci., Cambridge, Mass., 1989.

Bai, Q., and D. L. Kohlstedt, Substantial hydrogen solubility in olivine and implications for water storage in the mantle, *Nature, 357*, 672-674, 1992.

Bell, D. R., and G. R. Rossman, Water in the Earth's mantle: The role of nominally anhydrous minerals, *Science, 255*, 1391-1397, 1992.

Bullard, E.C., and R.L. Parker, Electromagnetic induction in the oceans, in *The Sea,* vol. 4, Part 1, edited by A.D. Maxwell, pp. 695-730, Wiley-Interscience, New York, 1968.

Cara, M. and J. J. Leveque, Anisotropy of the asthenosphere: The higher mode data of the Pacific revisited, *Geophys. Res. Lett., 15*, 205-208, 1988.

Chave, A. D. and D. S. Luther, Low-frequency, motionally induced electromagnetic fields in the ocean, *J. Geophys. Res., 95*, 7185-7200, 1990.

Chave, A. D., and J. T. Smith, On electric and magnetic galvanic distortion tensor decomposition, *J. Geophys. Res., 99*, 4669-4682, 1994.

Chave, A. D., and D. J. Thomson, Some comments on magnetotelluric response function estimation, *J. Geophys. Res., 94,* 14,215-14,225, 1989.

Chave, A. D., R P. Von Herzen, K. A. Poehls, and C. S. Cox, Electromagnetic induction fields in the deep ocean north-east of Hawaii: Implications for mantle conductivity and source fields, *Geophys. J. R. Astron. Soc., 66*, 379-406, 1981.

Chave, A. D., D.J. Thomson, and M. E. Ander, On the robust estimation of power spectra, coherences, and transfer functions, *J. Geophys. Res., 92*, 633-648, 1987.

Chave, A. D., A. H. Flosadóttir, and C. S. Cox, Some comments on seabed propagation of ULF/ELF electromagnetic fields, *Radio Sci. 25, 825-836,* 1990.

Chave, A. D., D. S. Luther, L. J. Lanzerotti, and L. V. Medford, Geoelectric field measurements on a planetary scale: Oceanographic and geophysical applications, *Geophys. Res. Lett., 19,* 1411-1414, 1992.

Chekhmir, A. S., and M. B. Epel'baum, Diffusion in magmatic melts: New study, in *Structure and Properties of Silicate Melts*, edited by B. O. Mysen, pp. 99-119, Elsevier, New York, 1988.

Constable, S. C., Conduction by mantle hydrogen, *Nature, 362*, 704, 1993.

Constable, S. C., and G. Heinson, In defense of a resistive oceanic upper mantle: Reply to a comment by Tarits, Chave and Schultz, *Geophys. J. Int., 114*, 717-723, 1993.

Constable, S. C., T. J. Shankland, and A. Duba, The electrical conductivity of an isotropic olivine mantle, *J. Geophys. Res., 97*, 3397-3404, 1991.

Cox, C. S., S. C. Constable, A. D. Chave, and S. C. Webb, Controlled-source electromagnetic sounding of the oceanic lithosphere, *Nature, 320*, 52-54, 1986.

Duba, A., and S. Constable, The electrical conductivity of lherzolite, *J. Geophys. Res., 98*, 11,885-11,899, 1993.

Egbert, G. D., Noncausality of the discrete-time magnetotelluric impulse response, *Geophysics, 57*, 1354-1358, 1992.

Egbert, G. D., and J. R. Booker, Multivariate analysis of geomagnetic array data, 1, The response space, *J. Geophys. Res., 94*, 14,227-14,247, 1989.

Egbert, G. D., and J. R. Booker, Very long period magnetotellurics at Tucson Observatory: Implications for mantle conductivity, *J. Geophys. Res., 97*, 15,099-15,112, 1992.

Egbert, G. D., J. R. Booker, and A. Schultz, Very long period magnetotellurics at Tucson Observatory: Estimation of impedances, *J. Geophys. Res., 97*, 15,113-15,128, 1992.

Everett, M. E., and A. Schultz, Two-dimensional nonlinear magnetotelluric inversion using a genetic algorithm, *J. Geomagn. Geoelectr., 45*, 1013-1026, 1993.

Filloux, J. H., Magnetotelluric soundings over the northeast Pacific may reveal spatial dependence of depth and conductance of the asthenosphere, *Earth Planet. Sci. Lett., 46*, 244-252, 1980.

Forsyth, D. W., The early structural evolution and anisotropy of the oceanic upper mantle, *Geophys. J. R. Astron. Soc., 43*, 103-162, 1975.

Forsyth, D. W., Geophysical constraints on mantle flow and melt generation beneath mid-ocean ridges, in *Mantle Flow and Melt Generation at Mid-Ocean Ridges, Geophys. Monogr. Ser.*, vol.71, edited by J. Phipps Morgan, D. K. Blackman, and J. M. Sinton, pp. 1-65, AGU, Washington, D. C., 1992.

Gasparik, T., The role of volatiles in the transition zone, *J. Geophys. Res., 98*, 4287-4299, 1993.

Gough, D. I., Magnetometer array studies, earth structure, and tectonic processes, *Rev. Geophys., 27*, 141-157, 1989.

Grand, S. P., and D. V. Helmberger, Upper mantle shear structure of North America, *Geophys. J. R. Astron. Soc., 76*, 399-438, 1984.

Hashin, Z., and S. Shtrikman, A variational approach to the theory of effective magnetic permeability of multiphase materials, *J. Appl. Phys., 33*, 3125-3131, 1962.

Heinson, G., and S. Constable, The electrical conductivity of the oceanic upper mantle, *Geophys. J. Int., 110*, 159-179, 1992.

Jones, A. G., A. D. Chave, G. Egbert, D. Auld, and K. Bahr, A comparison of techniques for magnetotelluric response function estimation, *J. Geophys. Res., 94*, 14201-14213, 1989.

Jordan, T. H., Continents as a chemical boundary layer, *Philos. Trans. R. Soc. London., A 301*, 359-373, 1981.

Karato, S., The role of hydrogen in the electrical conductivity of the upper mantle, *Nature, 347*, 272-273, 1990.

Keppler, H., and N. S. Bagdassarov, High temperature FTIR spectra of H_2O in rhyolite melt to 1300°C, *Am. Mineral., 78*, 1324-1327, 1993.

Kittel, C., *Introduction to Solid State Physics*, John Wiley, New York, 1957.

Kohlstedt, D. L., H. Keppler, and D. C. Rubie, Solubility of water in α, β and γ $(Mg,Fe)_2SiO_4$ at high pressures, *Eos Trans. AGU, 75* (44), Fall Meet. Suppl., 652, 1994.

Kurtz, R. D., J. M. DeLaurier, and J. C. Gupta, The electrical conductivity distribution beneath Vancouver Island: A region of active subduction, *J. Geophys. Res., 95*, 10929-10946, 1990.

Lanzerotti, L. J., C.H. Sayres, L. V. Medford, J. S. Kraus, and C. G. Maclennan, Earth potential over 4000 km between Hawaii and California, *Geophys. Res. Lett., 19*, 1177-1180, 1992.

Larsen, J. C., An introduction to electromagnetic induction in the ocean, *Phys. Earth Planet. Inter., 7*, 389-398, 1970.

Larsen, J. C., Removal of local surface conductivity effects from low frequency mantle response curves, *Acta Geod. Geophys. Montanistica Acad. Sci. Hung., 12*, 183-186, 1977.

Li, X., and R. Jeanloz, Phase identification and electrical conductivity of an H_2O-bearing silicate assemblage at lower mantle conditions, *Nature, 350*, 332-333, 1991.

Mackie, R. L., G. R. Bennett, and T. R. Madden, Long-period magnetotelluric measurements near the central California coast: A land-locked view of the conductivity structure under the Pacific Ocean, *Geophys. J., 95*, 181-194, 1988.

Mackwell, S. J., and D. L. Kohlstedt, Diffusion of Hydrogen in olivine: Implications for water in the mantle, *J. Geophys. Res., 95*, 5079-5088, 1990.

Madden, T. R., Transmission systems and network analogies to geophysical forward and inverse problems, *ONR Tech. Rep. 72-3*, Off. of Nav. Res., Arlington, Va., 1972.

McKenzie, D. P., Some remarks on the movement of small melt fractions in the mantle, *Earth Planet. Sci. Lett., 74*, 81-91, 1985.

Michael, P. J., The concentration, behavior and storage of H_2O in the suboceanic upper mantle: Implications for mantle metasomatism, *Geochim. Cosmochim. Acta, 52*, 555-566, 1988.

Navrotsky, A., and K. Bose, Hydrous phases may be stable into the transition zone, *Eos Trans. AGU, 75* (16), Spring Meet. Suppl., 230, 1994.

Nicolas, A., and N. I. Christensen, Formation of anisotropy in upper mantle peridotites: A review, in *Composition, Structure and Dynamics of the Lithosphere-Asthenosphere System, Geodyn. Ser.*, vol. 35, edited by K. Fucks and C. Froidevaux, pp. 111-123, AGU, Washington, D. C., 1987.

Nishimura, C. E., and D. W. Forsyth, The anisotropic structure of the upper mantle in the Pacific, *Geophys. J., 96*, 203-229, 1989.

Nolet, G., and A. Zielhuis, Low *S* velocities under the Tornquist-Teisseyre zone: Evidence for water injection into the transition zone by subduction, *J. Geophys. Res., 99*, 15,813-15,820, 1994.

Park, S. K., G. P. Biasis, R. L. Mackie, and T. R. Madden, Magnetotelluric evidence for crustal suture zones bounding the southern great valley, California, *J. Geophys. Res., 96*, 353-376, 1991.

Parker, R. L., The inverse Problem of electromagnetic induction: Existence and construction of solutions based on incomplete data, *J. Geophys. Res., 85*, 4421-4428, 1980.

Parker, R. L., and K. A. Whaler, Numerical methods for establishing solutions to the inverse problem of electromagnetic induction, *J. Geophys. Res., 86*, 9574-9584, 1981.

Parmentier, E. M., and J. Phipps Morgan, Spreading rate dependence of three-dimensional structure in oceanic spreading centers, *Nature, 348*, 325-328, 1990.

Parson, B., and J. G. Sclater, An analysis of the variation of ocean floor bathymetry and heat flow with age, *J. Geophys. Res., 82*, 803-827, 1977.

Ranganayaki, R.P., and T.R. Madden, Generalized thin sheet analysis in magnetotellurics: An extension of Price's analysis, *Geophys. J. R. Astron. Soc., 60*, 445-457, 1980.

Revenaugh, J., and S. A. Sipkin, Seismic evidence for silicate melt atop the 410-km mantle discontinuity, *Nature, 369*, 474-476, 1994.

Salters, V. J. M., and S. R. Hart, The hafnium paradox and the role of garnet in the source of mid-ocean ridge basalts, *Nature, 342*, 420-422, 1989.

Schmeling, H., Numerical models on the influence of partial melt on elastic, anelastic, and electrical properties of rocks, II, Electrical conductivity, *Phys. Earth Planet. Inter., 43, 123-136*, 1986.

Schock, R.N., A.G. Duba, and T.J. Shankland, Electrical conduction in olivine, *J. Geophys. Res., 94*, 5829-5839, 1989.

Schultz, A., On the vertical gradient and associated heterogeneity in mantle electrical conductivity, *Phys. Earth Planet. Inter., 64*, 68-86, 1990.

Schultz, A., and J. Larsen, Analysis of zonal field morphology and data quality for a global set of magnetic observatory daily mean values, *J. Geomagn. Geoelectr., 35*, 835-846, 1983.

Schultz, A., and J. Larsen, On the electrical conductivity of the mid-mantl, II, Delineation of heterogeneity by application of extremal inverse solutions, *Geophys. J. Int., 101*, 565-580, 1990.

Schultz, A., R. D. Kurtz, A. D. Chave, and A. G. Jones, Conductivity discontinuities in the upper mantle beneath a stable craton, *Geophys. Res. Lett., 20*, 2941-2944, 1993.

Shankland, T. J., and A. G. Duba, Standard electrical conductivity of isotropic, homogeneous olivine in the temperature range 1200°-1500°C, *Geophys. J. Int., 103*, 25-31, 1990.

Smith, J. T., and J. R. Booker, Magnetotelluric inversion for minimum structure, *Geophysics, 53*, 1565-1576, 1988.

Tarits, P., A. D. Chave, and A. Schultz, Comment on 'The electrical conductivity of the oceanic upper mantle' by G. Heinson and S. Constable, *Geophys. J. Int., 114*, 711-716, 1993.

Thompson, A. B., Water in the Earth's upper mantle, *Nature, 358*, 295-302, 1992.

Thomson, D. J., Spectrum estimation techniques for characterization and development of WT4 waveguide, I, *Bell Syst. Tech. J., 56*, 1769-1815, 1977.

Thomson, D. J., Spectrum estimation and harmonic analysis, *Proc. IEEE, 70,* 1055-1096, 1982.

Thomson, D. J., and A. D. Chave, Jackknifed error estimates for spectra, coherences, and transfer functions, in *Advances in Spectrum Analysis and Array Processing,* vol. 1, edited by S. Haykin, pp. 58-113, Prentice-Hall, Englewood Cliffs, N.J., 1991.

Tyburczy, J. A., and H. S. Waff, Electrical conductivity of molten basalt and andesite to 25 kilobars pressure: Geophysical significance and implications for charge transport and melt structure, *J. Geophys. Res., 88,* 2413-2430, 1983.

Waff, H. S., Theoretical considerations of electrical conductivity in a partially molten mantle and implications for geothermometry, *J. Geophys. Res., 79*, 4003-4010, 1974.

Walker, D., C. B. Agee, and Y. Zhang, Fusion curve slope and crystal/liquid buoyancy, *J. Geophys. Res., 93*, 313-323, 1988.

Wannamaker, P. E., J. R. Booker, A. G. Jones, A. D. Chave, J. H. Filloux, H. S. Waff, L. K. Law, and C. T. Young, Conductivity cross section through the Juan de Fuca subduction system and its tectonic implications, *J. Geophys. Res., 94*, 14,127-14,144, 1989.

Watson, E. B., Diffusion of cesium ions in H_2O-saturated granitic melt, *Science, 205*, 1259-1260, 1979.

Watson, E. B., Diffusion in magmas at depth in the Earth: The effects of pressure and dissolved H_2O, *Earth Planet. Sci. Lett.*, 52, 291-301, 1981.

Young, T. E., H. W. Green II, A. M. Hofmeister, and D. Walker, Infrared spectroscopic investigation of hydroxyl in β-$(Mg,Fe)_2SiO_4$ and coexisting olivine: Implications for mantle evolution and dynamics, *Phys. Chem. Miner., 19*, 409-422, 1993.

A. Chave, G. Hirth, and D. Lizarralde, Woods Hole Oceanographic Institution, Woods Hole, MA 02543. (e-mail: danl@azure.whoi.edu)

A. Schultz, Institute of Theoretical Geophysics, University of Cambridge, CB2 3EQ, England.

(Received October 10, 1994; revised April 6, 1995;
accepted April 11, 1995.)